

Thickness-dependent structural stability and transition in molybdenum disulfide under hydrostatic pressure

Jiansheng Dong(董健生), Gang Ouyang(欧阳钢)
Citation: Chin. Phys. B . 2020, 29(8): 086403 . **doi:** 10.1088/1674-1056/ab9440
Journal homepage: http://cpb.iphy.ac.cn; http://iopscience.iop.org/cpb

What follows is a list of articles you may be interested in

High pressure and high temperature induced polymerization of C_{60} quantum dots

Shi-Hao Ruan(阮世豪), Chun-Miao Han(韩春淼), Fu-Lu Li(李福禄), Bing Li(李冰), Bing-Bing Liu(刘冰冰)
Chin. Phys. B . 2020, 29(2): 026402 . **doi:** 10.1088/1674-1056/ab6657

Semiconductor-metal transition in GaAs nanowires under high pressure

Yi-Lan Liang(梁艺蓝), Zhen Yao(姚震), Xue-Tong Yin(殷雪彤), Peng Wang(王鹏), Li-Xia Li(李利霞), Dong Pan(潘东), Hai-Yan Li(李海燕), Quan-Jun Li(李全军), Bing-Bing Liu(刘冰冰), Jian-Hua Zhao(赵建华)
Chin. Phys. B . 2019, 28(7): 076401 . **doi:** 10.1088/1674-1056/28/7/076401

Pressure-induced isostructural phase transition in α-$Ni(OH)_2$ nanowires

Xin Ma(马鑫), Zhi-Hui Li(李志慧), Xiao-Ling Jing(荆晓玲), Hong-Kai Gu(顾宏凯), Hui Tian(田辉), Qing Dong(董青), Peng Wang(王鹏), Ran Liu(刘然), Bo Liu(刘波), Quan-Jun Li(李全军), Zhen Yao(姚震), Bing-Bing Liu(刘冰冰)
Chin. Phys. B . 2019, 28(6): 066402 . **doi:** 10.1088/1674-1056/28/6/066402

Surface stabilized cubic phase of $CsPbI_3$ and $CsPbBr_3$ at room temperature

Feng Yang(杨凤), Cong Wang(王聪), Yuhao Pan(潘宇浩), Xieyu Zhou(周谐宇), Xianghua Kong(孔祥华), Wei Ji(季威)
Chin. Phys. B . 2019, 28(5): 056402 . **doi:** 10.1088/1674-1056/28/5/056402

Anomalous behavior and phase transformation of α -GaOOH nanocrystals under static compression

Zhao Zhang(张钊), Hang Cui(崔航), Da-Peng Yang(杨大鹏), Jian Zhang(张剑), Shun-Xi Tang(汤顺熙), Si Wu(吴思), Qi-Liang Cui(崔啟良)
Chin. Phys. B . 2017, 26(10): 106402 . **doi:** 10.1088/1674-1056/26/10/106402

Thickness-dependent structural stability and transition in molybdenum disulfide under hydrostatic pressure*

Jiansheng Dong(董健生) and Gang Ouyang(欧阳钢)†

Key Laboratory of Low-Dimensional Quantum Structures and Quantum Control of Ministry of Education, Key Laboratory for Matter Microstructure and Function of Hunan Province, Synergetic Innovation Center for Quantum Effects and Applications (SICQEA), Hunan Normal University, Changsha 410081, *China*

(Received 3 February 2020; revised manuscript received 19 April 2020; accepted manuscript online 19 May 2020)

Understanding the physical mechanism of structural stability and transition in various polytypes of layered transition metal dichalcogenides under the external stimulus is of crucial importance for their new applications. Here, we investigate the thickness-dependent structural properties of MoS_2 under the condition of hydrostatic pressure in terms of bond relaxation and thermodynamics considerations. For both types of MoS_2structures, we find that the transition and metallization are significantly modulated by hydrostatic pressure and the number of layers. We establish a pressure-size phase diagram to address the transition mechanism. Our study not only provides insights into the thickness-dependent structural properties of MoS_2, but also shows a theoretical guidance for the design and fabrication of MoS_2-based devices.

Keywords: bond relaxation, thickness effect, layered transition metal dichalcogenides, structural transition, pressure modulation

PACS: 64.70.Nd, 61.50.Ks, 64.10.+h, 64.60.an **DOI:** 10.1088/1674-1056/ab9440

1. Introduction

The emergence of two-dimensional transition metal dichalcogenides (2D-TMDs) offers exciting opportunities for probing new physical phenomena and potential applications in catalysis,[1,2] optoelectronics,[3,4] nanoelectronics,[5–7] etc. For example, Maeso *et al.*[4] recently investigated the electrical and optical properties of vertical few-layer MoS_2 and found that the light absorption can be improved by fabricating vertical photodevices using few-layer flakes, achieving a photoresponse up to 0.11 $A{\cdot}W^{-1}$ and an external quantum efficiency up to 30%. Shahraki *et al.*[6] reported that MoS_2 multilayers have unique mechanical and electrical properties, which can be a promising channel material for the n-type piezoelectric field-effect transistor. However, considering that the devices constructed of TMDs are often worked under various environments,[8–12] it is necessary to explore the change of related material properties under the external stimulus.

In particular, external pressure provides a viable avenue to modulate the crystal structure and electronic properties in a clean and precisely controllable manner. Currently, a series of experiments[13–19] and theories[20–22] showed that the phase transition of $2H_c$-to-$2H_a$ and metallization in MoS_2 can be induced by hydrostatic pressure. Especially, the exciting properties of pressure-induced superconductivity emerged in $2H_a$-MoS_2 and proved that $2H_a$-MoS_2 is a high-pressure stable phase,[23] while the phase transition of $2H_c$-to-$2H_a$ is absent in $MoSe_2$, $MoTe_2$, and WS_2 under the condition of hydrostatic pressure.[22,24–27] Therefore, it is an urgent issue to explore the pressure-dependent phase transition of MoS_2 from $2H_c$-to-$2H_a$. For the case of bulk MoS_2, many experimental measurements showed the transition of $2H_c$-to-$2H_a$, associating with a semiconducting-to-metallic state, but there are large differences in the values of transition pressure measured by different experimental groups (18.5–26 GPa).[13–19] Also, the structural transition of $2H_c$-to-$2H_a$ and metallization in bulk MoS_2 under pressure have been reported by using first-principle calculations and molecular dynamics simulations and the values of pressure are in the range of 13 GPa to 20 GPa.[13,20–22] In addition, the transition pressure of MoS_2 from $2H_c$-to-$2H_a$ under hydrostatic pressure increases from 19.0 GPa to 36.0 GPa as the thickness reduces from bulk to bilayer.[19] Meanwhile, MoS_2 undergoes a metallization transition upon hydrostatic pressure, while the transition pressure decreases as the number of layers increases.[28,29] However, there are great differences (13–26 GPa) in transition pressure between some experiments and theories for MoS_2. Furthermore, the potential mechanisms of structural transition, pressure metallization, and related evolution in MoS_2 have not been comprehensively understood. In particular, the pressure-size phase diagram is still unclear.

In this paper, we investigate the structural transition and metallization of MoS_2 under pressure based on the bond relaxation method and thermodynamics. It is found that the transition pressures of $2H_c$-to-$2H_a$ and metallization increase significantly with a decreasing number of layers, while the change rate of structural transition is greater than that of metallization. Moreover, we establish a size-pressure phase diagram of MoS_2, identifying the transition mechanism of the structural properties.

*Project supported by the National Natural Science Foundation of China (Grant No. 91833302).

†Corresponding author. E-mail: gangouy@hunnu.edu.cn

© 2020 Chinese Physical Society and IOP Publishing Ltd

2. Theoretical model

MoS_2 consists of intralayer strong covalent bonding and is stacked with interlayer by weak vdW bonding. Noticeably, the structural transition of $2H_c$-to-$2H_a$ originates from the interlayer sliding. Conventionally, the Gibbs free energy $G_{sum}(P)$ of MoS_2 under hydrostatic pressure is $G_{sum}(P) = G_0 + G(P)$, where G_0 is a reference value at ambient pressure, and $G(P)$ is a part of the pressure-induced energy storage of unit cell. Since $G(P) = -\int S\,dT + \int V\,dP$ and the temperature is almost unchanged under the approach of pressure, the equation can be simplified into $G(P) = \int V\,dP$.

Under the condition of hydrostatic pressure, the lattice strain can be expressed as $\varepsilon(x,y,z) = l/l_0 - 1$, where l and l_0 denote the length after and before relaxation along x-, y-, and z-directions. For the intralayer of $2H_c$ and $2H_a$ phases, it is feasible to take the elastic modulus as a constant in a small strain range due to the strong ionic-covalent bonds, while assuming that sliding of interlayer does not change the properties with intralayer.[30,31] Therefore, the pressure-dependent strain of intralayer along with x-, y-, and z-directions can be shown as

$$\begin{cases} \varepsilon_x = P\left(1/Y_x - v_{\parallel}/Y_y - v_{\perp}/Y_z\right), \\ \varepsilon_y = P\left(1/Y_y - v_{\parallel}/Y_x - v_{\perp}/Y_z\right), \\ \varepsilon_z = P\left(1/Y_z - v_{\parallel}/Y_x - v_{\parallel}/Y_y\right), \end{cases} \tag{1}$$

where Y_x, Y_y, and Y_z are the elastic moduli of intralayer along x-, y-, and z-directions. $v_{\parallel}$ and $v_{\perp}$ are the in-plane and out-of-plane Poisson's ratios, respectively. It should be noted that the elastic moduli in x-, y-, z-directions are 200.3 GPa, 197.8 GPa, and 511 GPa and the in-plane and out-of-plane Poisson's ratios are 0.21 and 0.27, respectively.[30,32–34] $\varepsilon_x = a/a_0 - 1$, $\varepsilon_y = b/b_0 - 1$, and $\varepsilon_z = c/c_0 - 1$, where a (b) and a_0 (b_0) are the strained and the equilibrium lattice parameters, respectively. c and c_0 correspond to the distances of S–S after and before being compressed. The bond length $d = \sqrt{\left(a/\sqrt{3}\right)^2 + (c/2)^2}$, and bond angles $\cos\theta = 1 - \left(\frac{a}{2d}\right)^2$ and $\cos\psi = 1 - \left(\frac{c}{2d}\right)^2$.

In general, the interlayer interactions of the adjacent layers in MoS_2 include three kinds of modes, i.e., S–S, S–Mo, and Mo–Mo, and the interaction can be described by the Lenard-Jones potential, i.e., $U(r) = -\Gamma\left[(\sigma/r_{ij})^{12} - (\sigma/r_{ij})^6\right]$, where r_{ij} denotes the distance between i and j atoms. $(\sigma/r_{ij})^{12}$ and $(\sigma/r_{ij})^6$ are the pairwise repulsion and attraction, respectively. For the nearest-neighbor interaction, the equilibrium spacing r_0 is related to σ as $r_0^6 = 2\sigma^6$.[32,35] Γ corresponds to the depth of the energy well at the equilibrium separation.[32,36] In our case, we take $\Gamma(\sigma)$ of S–S, S–Mo, and Mo–Mo as 0.024 eV (3.13 Å), 0.0028 eV (3.67 Å), and 0.00059 eV (4.20 Å), respectively.[32,35,36] The total van der Waals (vdW) interaction energy can be written as $U_{vdW} = \frac{1}{2}\sum_{i,j}\sum_{i,j} U(r)$. Moreover, the average interlayer interaction of unit cell for two phases of $2H_c$ and $2H_a$ through taking into account of the nearest neighbor atoms is

$$\begin{aligned} U_{vdW}(\varphi = 2H_c, 2H_a) = {} & \rho^{\varphi}_{S-S}\Gamma_{S-S}\left[\left(\frac{\sigma_{S-S}}{r_{S-S}}\right)^{12} - \left(\frac{\sigma_{S-S}}{r_{S-S}}\right)^{6}\right] \\ & + \rho^{\varphi}_{S-Mo}\Gamma_{S-Mo}\left[\left(\frac{\sigma_{S-Mo}}{r_{S-Mo}}\right)^{12} - \left(\frac{\sigma_{S-Mo}}{r_{S-Mo}}\right)^{6}\right] \\ & + \rho^{\varphi}_{Mo-Mo}\Gamma_{Mo-Mo}\left[\left(\frac{\sigma_{Mo-Mo}}{r_{Mo-Mo}}\right)^{12} - \left(\frac{\sigma_{Mo-Mo}}{r_{Mo-Mo}}\right)^{6}\right], \end{aligned} \tag{2}$$

where ρ^{φ}_{S-S}, ρ^{φ}_{S-Mo}, and ρ^{φ}_{Mo-Mo} are the numbers of atom interaction in the unit cell. For the case of $2H_c$-MoS_2, $\rho^{\varphi}_{S-S} = 6$, $\rho^{\varphi}_{S-Mo} = 4$, $\rho^{\varphi}_{Mo-Mo} = 3$, $r_{S-S} = \sqrt{t_1^2 + \frac{\sqrt{3}}{3}a^2}$, $r_{S-Mo} = t_1 + \frac{c}{2}$, and $r_{Mo-Mo} = \sqrt{(t_1 + c)^2 + \frac{\sqrt{3}}{3}a^2}$. While for $2H_a$-MoS_2, $\rho^{\varphi}_{S-S} = 6$, $\rho^{\varphi}_{S-Mo} = 6$, $\rho^{\varphi}_{Mo-Mo} = 2$, $r_{S-S} = \sqrt{t_2^2 + \frac{\sqrt{3}}{3}a^2}$, $r_{S-Mo} = \sqrt{\left(t_2 + \frac{c}{2}\right)^2 + \frac{\sqrt{3}}{3}a^2}$, and $r_{Mo-Mo} = t_2 + c$. t_1 and t_2 are the pressure-dependent interlayer separations of $2H_c$ and $2H_a$ phases, respectively. Conventionally, the equilibrium interlayer distance of the two phases can be obtained by $\partial U_{vdW}/\partial t|_{t=t_{01},t_{02}} = 0$, where t_{01} and t_{02} are the interlayer distances at ambient pressure. Also, the interlayer elastic modulus is described by the second derivative of the interlayer interaction energy, namely, $Y(t) = N_0 \cdot d^2U_{vdW}/dt^2$,[36] where $N_0 = 11$ nm^2 is the number of atoms. Thus, the strain in the interlayer under hydrostatic pressure can be obtained as

$$\varepsilon_t = -\frac{P}{Y(t)\cdot t_0} \tag{3}$$

where $\varepsilon_t = t/t_0 - 1$. $t$and $t_0$are the interlayer separations after and before being compressed in both $2H_c$ and $2H_a$ phases, respectively. Therefore, the pressure-dependent unit volume of bulk MoS_2 can be shown as $V(P) = a\cdot b\cdot(c+t)$. Combining with the above relationship, we obtain the relative Gibbs free energy of $2H_a$- and $2H_c$-MoS_2 in bulk, $\Delta G = (G_{02} - G_{01}) + \int_0^P ab(t_2 - t_1)\,dP$, where G_{01} and G_{02} are the energies of $2H_c$ and $2H_a$ phases at ambient pressure.

Generally, the thermal stability of a system is determined by the cohesive energy.[37,38] Moreover, the transition pressure (P_c) of the specimen correlates to the cohesive energy, i.e., $\langle P_c(D)\rangle \propto \left\langle \sum_{i\le 3} z_i E_i \right\rangle$, where z_i and E_i are the coordination number (CN) and the single bond energy for all atoms, respectively. D is the thickness of MoS_2. Clearly, the compression of the bond length and the bond strength will be stronger under the condition of pressure, resulting in the increasment of the transition pressure, while decreasing thickness leads to the reduction of the transition pressure because of the lower cohesive energy.[38,40] Therefore, the competition between energy enhancement induced by external pressure and reduction driven by the thickness down to nanoscale determines the transition pressure.

In the case of pressure, the entire atomic bonds of the specimen become shorter and stronger because of volume

shrinkage and deformation energy storage. Therefore, according to the integral of the volume-pressure profile, the pressure-induced energy storage is

$$\begin{aligned}\Delta E &= \int_0^{P_c} V\,\mathrm{d}P = V_0\int_0^{P_c}\left(1+\int_0^{P_c}\beta\,\mathrm{d}P\right)\mathrm{d}P \\ &\approx V_0P_c\left(1+\beta P_c/2\right) = \sum_{i\le 3} z_i\left(\Delta E_i\right) \propto \Delta P_c,\end{aligned} \tag{4}$$

where $\beta = \mathrm{d}V/(V_0\,\mathrm{d}P)$ and equals to the inverse of bulk modulus. The approximation of $V = V_0\left(1+\int_0^{P_c}\beta\,\mathrm{d}P\right) \cong V_0\left(1+\beta P_c\right)$ can be as a constant. Therefore, the relative change of transition pressure is

$$\frac{\Delta P_c\left(P_{cD}\right)}{P_{cb}} = \frac{P_{cD}\left(1+\beta P_{cD}/2\right)}{P_{cb}\left(1+\beta P_{cb}/2\right)} - 1, \tag{5}$$

where P_{cD} and P_{cb} are the transition pressures of the film and the bulk counterparts, respectively.

In addition, in light of the atomic-bond-relaxation (ABR) method,[41,42] the atoms located at the edge will relax spontaneously. Therefore, the intra-atomic potential well depresses from E_b to $E_i = c_i^{-m}E_b$, where E_b denotes the single bond energy of the bulk counterpart, and the index m is the bond nature factor. $c_i = 2/\left(1+\exp\left(\left(12-z_i\right)/8z_i\right)\right)$ is the bond contraction coefficient.[41,42] Thus, the thickness-dependent transition pressure is

$$\frac{\Delta P_c\left(D\right)}{P_c\left(\infty\right)} = \sum_{i\le 3}\gamma_i\left(z_{ib}c_i^{-m}-1\right), \tag{6}$$

where $z_{ib} = z_i/z_b$. $\gamma_i = \sum_{i\le 3} 2c_id_0/D$ is the surface-to-volume (SVR). Combining the pressure-induced magnifying and thickness-induced decreasing of the transition pressure, we obtain

$$\frac{\Delta P_c\left(D,P_{cD}\right)}{P_c\left(\infty,P_{cb}\right)} = \frac{P_{cD}\left(1+\beta P_{cD}/2\right)}{P_{cb}\left(1+\beta P_{cb}/2\right)} - 1 + \sum_{i\le 3}\gamma_i\left(z_{ib}c_i^{-m}-1\right). \tag{7}$$

On the other hand, the variation of the bond parameters in MoS_2 would induce the change of the system energy, and the interaction potential of intralayer consists of bond-stretching energy U_{bond}, bond angle variation energy U_{angle}, and Coulomb electrostatic energy U_{coul},[43,44]

$$U_{intra} = \sum U_{bond} + \sum U_{angle} + \sum U_{coul}. \tag{8}$$

Here $U_{bond} = D_0\times\left[1-\mathrm{e}^{-\alpha(d-d_0)}\right]^2$, $U_{angle} = \frac{1}{2}k_\theta\theta^2 + \frac{1}{2}k_\psi\psi^2$, $U_{coul} = C\cdot\frac{q_iq_j}{d}$, where D_0, α, k_θ, and k_ψ are the bond potential parameters. The values of D_0, α, k_θ, and k_ψ are 19.945, 0.858, 0.9387, and 0.8631.[43,44] q_i and q_j are the partial electrostatic charges, which are $0.76e$ and $-0.38e$ for Mo and S atoms, respectively.

Combining the interaction potentials of intralayer and interlayer, the pressure-induced variation of the average single bond energy in MoS_2 can be shown as $\Delta E_P = \Delta U_{intra} + (n-1)\,\Delta U_{inter}^{i=1,2}/3n$, where ΔU_{intra} is the single bond energy variation of the intralayer, and $\Delta U_{inter}^{i=1,2}$ is the interlayer interaction of an S atom. The superscripts 1 and 2 of the interlayer energy represent the $2H_c$ and $2H_a$ phases, respectively. Thus, the cohesive energy of the system under the pressure is

$$E_C\left(D,P\right) = \sum_{i\le 3} N_iz_iE_i^S + z_bE_B\left(N-\sum_{i\le 3}N_i\right), \tag{9}$$

where $E_B = E_b + \Delta E_P$, and $E_i^S = E_i + \Delta E_P$. N_i and N correspond to the atomic number of the i^{th} surface layer and the total number of the system, respectively. Notably, the bandgap is proportional to the single bond energy, i.e., $E_g \propto \langle E_0\rangle = E_C/N\langle z\rangle$, where $\langle z\rangle = \sum_{i\le 3}\gamma_i\left(z_i-z_b\right)+z_b$ is the average CN.[41,42] Consequently, by combining with the relationship shown above, the thickness-dependent bandgap in MoS_2 under hydrostatic pressure is

$$E_g\left(D,P\right) = \frac{z_b}{\langle z\rangle}\left[\sum_{i\le 3}\gamma_i\left(z_{ib}c_i^{-m}-1\right)+1\right]E_g^{b1}, \tag{10}$$

where $z_{ib} = z_i/z_b$, and E_g^{b1} denotes the bandgap of bulk $2H_c$-MoS_2.

3. Results and discussion

For the case of $2H_c$-MoS_2, the Mo atoms in one sheet are on the top of the S atoms in the next, while there is a misalignment between S atoms of the adjacent layer for $2H_a$-MoS_2(Fig. 1(a)). It is found that increasing hydrostatic pressure leads to a decrease of the lattice parameter a (the bond length d) and an increase of the thickness of the intralayer (Fig. 1(b)). The variation trends of bond angle in the opposite directions are the consequence of changes from in-plane θ and out-of-plane ψ with increasing pressure (Fig. 1(c)). The changes of lattice parameter and bond length are approximately linear due to strong covalent bonding between the Mo and S atoms, while an expansion of intralayer with the pressure is due to the effect of negative Poisson's ratio. In light of the ABR consideration,[41,42] the interlayer distances are 2.99 Å and 3.05 Å for $2H_c$ and $2H_a$ phases at ambient pressure, respectively (the inset of Fig. 1(d)). In detail, the phase transition does not change the interaction of S–S, while the interaction distances of Mo–S and Mo–Mo have been changed. Therefore, the interlayer distance is determined by the interactions of Mo–S and Mo–Mo. However, the interactions of Mo–S and Mo–Mo are weak at the interlayer, resulting in a small difference between the two phases. Notably, the interlayer distance of MoS_2 decreases significantly and non-linearly with increasing pressure, reflecting that the interlayer is associated with weak vdW bonding (Fig. 1(d)). Importantly, the change rate decreases with reducing interlayer distance due to the strong vdW interaction caused by the reduction of the interlayer distance. Furthermore, the variation range of $2H_a$-MoS_2 is slightly larger than that of $2H_c$-MoS_2, suggesting that the stacking order affects the interlayer interaction. Evidently, the changes in bond parameters are consistent with the available results from experimental measurements and theoretical calculations.[21,45,46]

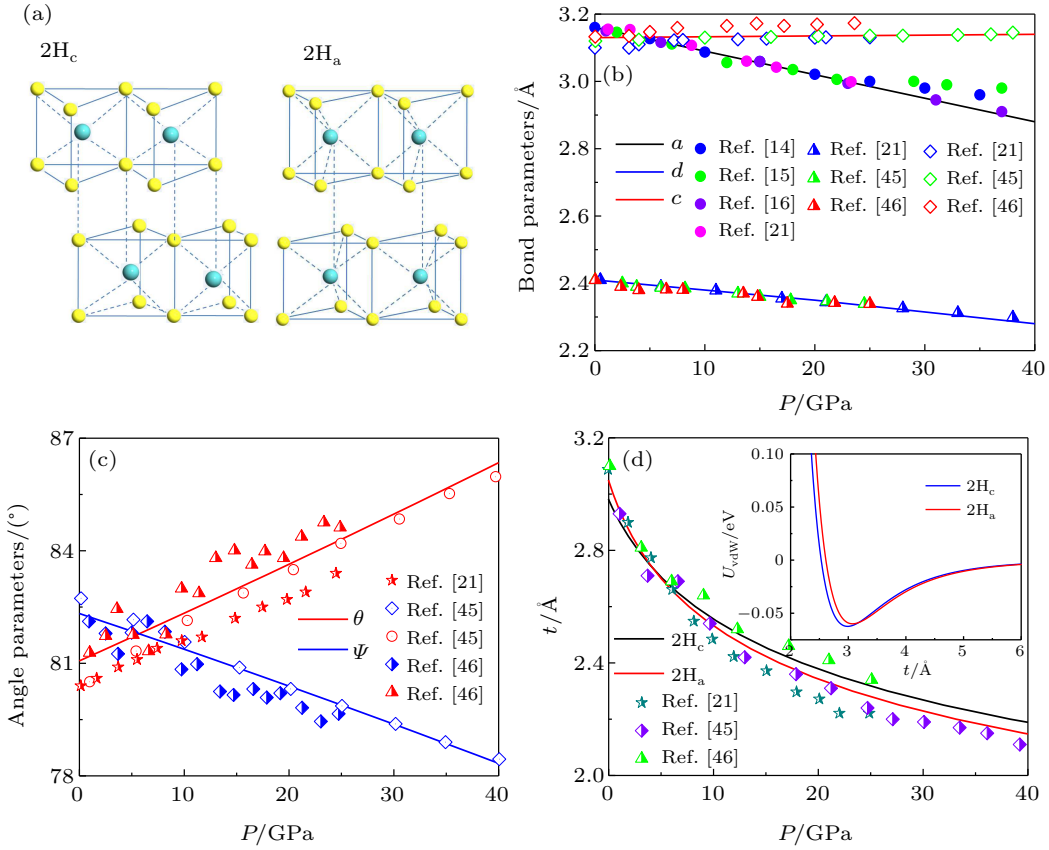


Fig. 1. (a) The schematic diagrams of atomic arrangement of $2H_c$- and $2H_a$-MoS_2 structures, where the Mo and S atoms are represented by blue and yellow balls, respectively. (b) Pressure-dependent variations of lattice parameter a, intralayer S–S distance c, and Mo–S bond length d. (c) Bond angles θ and ψ as a function of pressure. (d) Interlayer distance $t$as a function of pressure.

Figure 2(a) shows the relationship between pressure and unit volume of bulk MoS_2 in $2H_c$ and $2H_a$ phases. It is observed that the volume decreases gradually with increasing pressure and the volume of $2H_c$ is larger than that of $2H_a$ under high pressure as the variation of the volume is mainly contributed by the interlayer separation. In addition, fitting the curves of P–V by the third-order Birch–Murnaghan equation of state $P(V) = \frac{3B}{2}\left(\xi^{-7/3} - \xi^{-5/3}\right)\left\{1 + \frac{3}{4}\left(B' - 4\right)\left(\xi^{-2/3} - 1\right)\right\}$,[47,48] we obtain the bulk moduli of $2H_c$ and $2H_a$ phases as $B_0 = 76.06 \pm 0.11$ GPa ($B' = 3.12$ GPa) and $B_0 = 85.13 \pm 0.21$ GPa ($B' = 2.57$ GPa), respectively. The bulk moduli obtained in our studies are qualitatively in agreement with the results reported by Aksoy *et al.*[15] and Bandaru *et al.*[16] Figure 2(b) shows the pressure-dependent difference of Gibbs free energy of $2H_a$- to $2H_c$-MoS_2. The Gibbs free energies of the two phases cross near 20.6 GPa, indicating that the structural transition will take place. Notably, the large difference of transition pressure in some experiments may be due to two main factors: (1) different types of defects may appear in the samples, such as vacancies or dislocations, which affect the interlayer interaction; (2) different characterized methods, such as Raman spectra and x-ray diffraction, may lead to the differences.[14,17–19] In nature, reducing the size to nanoscale, the surface state of a nanomaterial is different from that of the bulk counterpart due to the low coordination numbers of the surface atoms, which infers that the transition pressure will be significantly affected by the surface effect. Figure 2(c) shows the layer-dependent transition pressure of MoS_2 from $2H_c$-to-$2H_a$. Clearly, the transition pressure is significantly enhanced from 20.6 GPa to 34.8 GPa as the thickness reduces from bulk to bilayer. Originally, the increase of the transition pressure can be attributed to the competition between pressure-induced enhancement and thickness-induced reduction of atomic cohesive energy. Similarly, Cheng *et al.*[19] demonstrated that the transition pressure of $2H_c$-to-$2H_a$ in MoS_2 can be continuously tuned from 19 GPa to 36 GPa by reducing the thickness from bulk down to bilayer by Raman analysis. As shown in the inset of Fig. 2(c), the phase transition from $2H_c$-to-$2H_a$ is through the sliding of the interlayer, which changes the stacking order of the adjacent layer. Generally, this structural transition is absent in the case of monolayer duo to lack of interlayer interaction.

Figure 3 depicts the pressure-dependent energy gain and band shift in MoS_2. Especially, the bond stretching and bond angle relaxation are monotonically decreasing, and the electrostatic interaction increases approximately linearly with increasing pressure, as shown in Fig. 3(a). It is obvious that the bond stretching energy and bond angle relaxation energy are negative, while the electrostatic interaction energy is positive. In addition, the interlayer interaction of S atom decreases ap-

proximately linearly with increasing pressure (Fig. 3(b)). Notably, the change rate of the interlayer interaction energy of $2H_a$ with increasing pressure is greater than that of $2H_c$. In general, when the system is perturbed by the external environment (such as doping and pressure), the system will relax to a new self-equilibrium state. In our case, the bandgap of bulk MoS_2 is red-shift with increasing pressure due to strong interlayer interactions and metallization at pressures of 23 GPa and 21 GPa for the $2H_c$ and $2H_a$ phases, respectively.

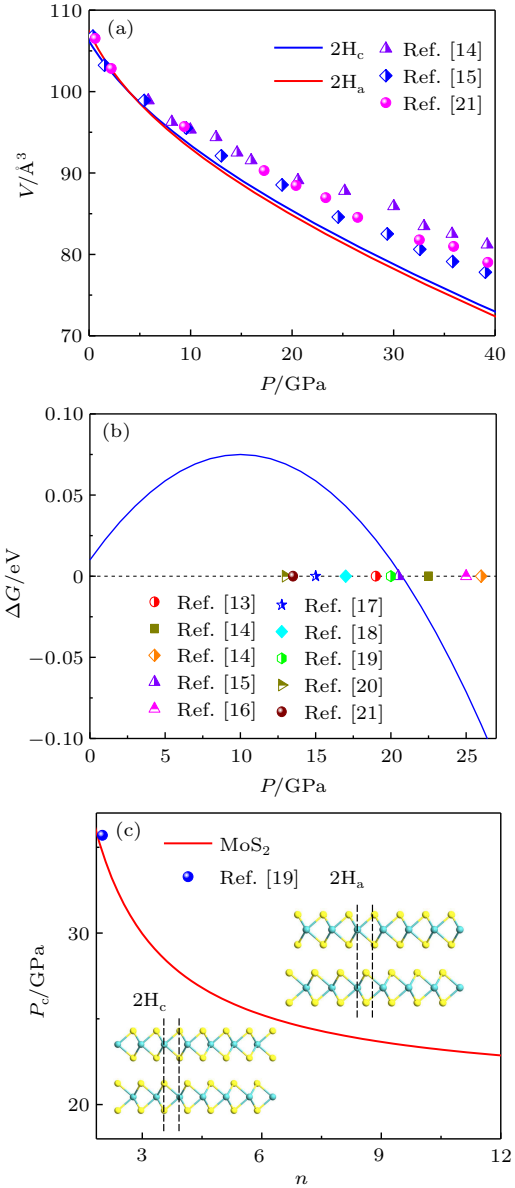


Fig. 2. (a) Pressure-dependent unit volume of MoS_2 in both $2H_c$ and $2H_a$ phases. (b) Pressure-dependent relative Gibbs free energy of $2H_a$- and $2H_c$-MoS_2 phases. (c) Phase diagram of MoS_2 from $2H_c$-to-$2H_a$ as a function of thickness. The solid line is the dividing line.

For the cases of monolayer and bilayer MoS_2, the bandgap blue-shifts first and then red-shifts with increasing pressure as shown in the inset of Fig. 3(c). In fact, the physical origin can be ascribed to the limited interlayer interaction and positive electrostatic interaction energy. Interestingly, the metallization of monolayer 2H-MoS_2 under pressure emerges at a pressure of 65.0 GPa, while for the bilayer MoS_2 with $2H_c$ and $2H_a$ phases, the metallization will be observed at 38.7 GPa and 37.9 GPa, respectively. Importantly, it can be clearly seen that the transition pressure of semiconductor-to-metal decreases as the number of layers increases and the metallization of the $2H_a$ phase is easier to achieve than that of the $2H_c$ phase (Fig. 3(c)). Similarly, Nayak *et al.*[28] and Kim *et al.*[29] found that the transition pressure decreases as the number of layers increases based on the density functional theory. Essentially, for 2H-MoS_2, the valence band maximum (VBM) and the conduction band minimum (CBM) are mainly dominated by the d orbitals of the Mo atoms and p orbitals of the S atoms. Under the

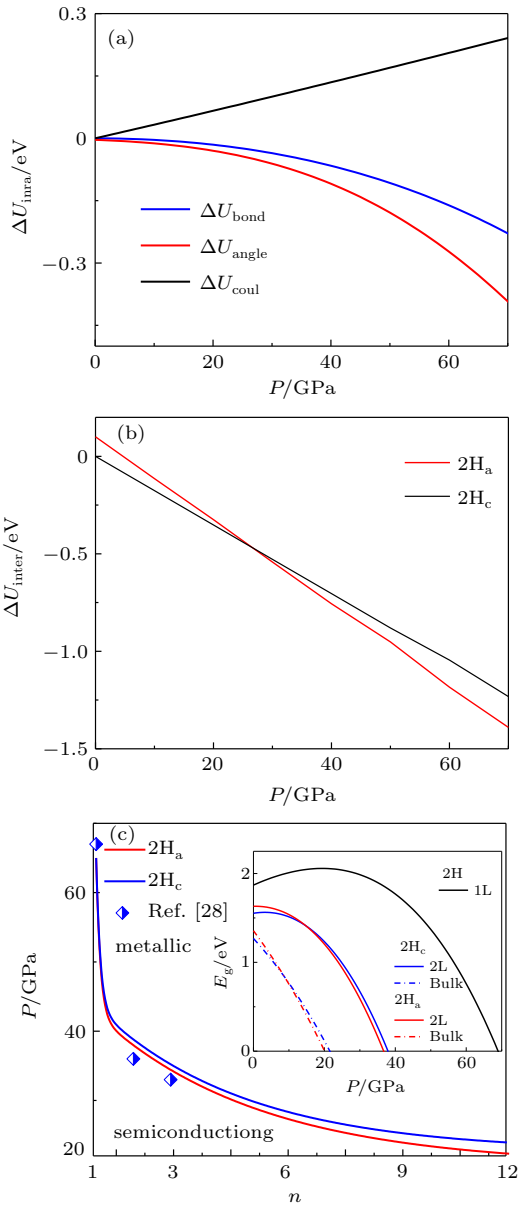


Fig. 3. (a) The pressure-dependent energy gain of single Mo–S bond including bond stretching, bond angle distortion, and electrostatic interaction energies. (b) The pressure-dependent interlayer interaction energy of an S atom in $2H_c$ and $2H_a$ phases. (c) The metallization transition of MoS_2 as a function of layer number. The solid line is the dividing line. The inset is the pressure-dependent bandgaps for monolayer, bilayer, bulk $2H_c$- and $2H_a$-MoS_2.

hydrostatic pressure, the strong hybridization between the d orbitals (mainly d_{z^2}, d_{xy}, and $d_{x^2-y^2}$) of Mo atoms and p orbitals of S atoms will result in the overlap between VBM and CBM as well as metallization.[28,29] Moreover, the stacking order between layers has a direct relationship with the transition pressure for MoS_2. Therefore, the system undergoes a series of phase transitions under pressure, which is from the semiconducting $2H_c$-to-$2H_a$ phases and to the metallic $2H_a$ phase with the pressure up to 70 GPa.

Based on the discussion mentioned above, we further establish a size-pressure phase diagram of 2H-MoS_2, as shown in Fig. 4. Also, we obtain the values of two types of phase transitions with different cases, which are in good agreement with the previous results (Table 1). Evidently, the sliding of interlayer takes place at the structural transition from $2H_c$-to-$2H_a$ and the transition pressure increases with a decreasing number of layers. In addition, the metallization arises from the overlap of CBM and VBM owing to the variation of the crystal potential induced by the change of bond identities. For multilayer and bulk MoS_2, the interlayer interaction is found to control the electronic structure, while for the case of monolayer MoS_2, the changes in the electronic structure under pressure are mainly controlled by the bond length and bond angle. Notably, for $n > 10$ layers, the structural transition and metallization in MoS_2 are almost complete simultaneously and the transition pressures are 20.6 GPa and 21 GPa, respectively. However, for $n < 10$ layers, the material becomes metallic when the structural transition is complete.

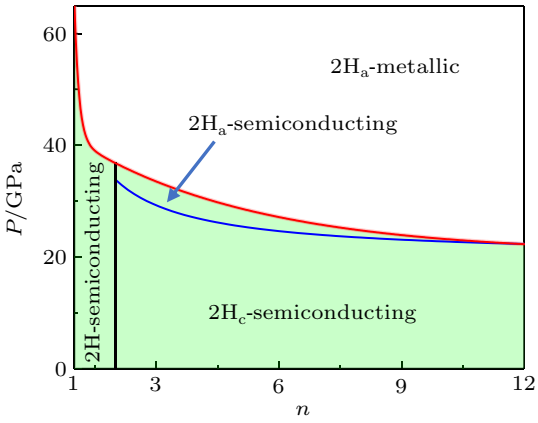


Fig. 4. Phase diagram of MoS_2 under the condition of hydrostatic pressure. The blue line represents the boundary between $2H_c$ and $2H_a$ phases. There is no interlayer interaction in monolayer represented by 2H phase. The semiconductor to metal transition is separated by the red line, while the pale green region denotes semiconducting.

Table 1. Calculated transition pressure (in GPa) of two types of phase transitions of MoS_2 for different cases.

Phase transition types		Monolayer	Bilayer	Trilayer	Bulk
$2H_c$-to-$2H_a$	our results	–	34.8	30.6	20.6
	previous results	–	36.0[d]	–	19.0[a], 23.0[b], 26.6[b], 20.5[c]
Semiconducting-to-metallic	our results	65.0	37.9	33.4	21.0
	previous results	67.9[e]	39.2[e]	29.5[e]	19.0[a], 22.3[e]

[a]Ref. [13], [b]Ref. [14], [c]Ref. [15], [d]Ref. [19], [e]Ref. [28].

4. Conclusion

In summary, we establish a theoretical model to investigate the structural properties of $MoS_2$by bond relaxation and thermodynamic considerations. We find that the structural transition of bulk MoS_2 from $2H_c$-to-$2H_a$ is determined by the interlayer coupling, while for the case of few-layers, the surface effect plays the dominant role in the transition pressure. The competition between energy enhancement induced by external pressure and reduction motivated by the thickness down to the nanoscale results in the significant transition pressure increase with decreasing thickness. Our predictions agree well with the available evidence, which suggests perspectives in a deep understanding and controlling structure design in two-dimensional materials.

References

[1] Chhowalla M, Shin H S, Eda G, Li L J, Loh K P and Zhang H 2013 *Nat. Chem.* **5** 263
[2] Tan C L and Zhang H 2015 *Chem. Soc. Rev.* **44** 2713
[3] Radisavljevic B, Radenovic A, Brivio J and Kis A 2011 *Nat. Nanotechnol.* **6** 147
[4] Maeso D, Gomez A C, Agraït N and Bollinger G R 2019 *Adv. Electron. Mater.* **5** 1900141
[5] Wang Q H, Kalantar-Zadeh K, Kis A, Coleman J N and Stranoet M S 2012 *Nat. Nanotechnol.* **7** 699
[6] Roldan R, Castellanos-Gomez A, Cappelluti E and Guinea F 2015 *J. Phys.: Condens. Matter.* **27** 313201
[7] Shahraki M A, Pourfath M, Member S and Esseni D 2019 *IEEE T. Electron. Dev.* **66** 1997
[8] Chen Y F, Xi J Y, Dumcenco D O, Liu Z, Suenaga K, Wang D, Shuai Z G, Huang Y S and Xie L M 2013 *ACS Nano* **7** 4610
[9] Liu K H, Zhang L M, Cao T, Jin C H, Qiu D N, Zhou Q, Zettl A, Yang P D, Louie S G and Wang F 2014 *Nat. Commun.* **5** 4966
[10] Huang Y P, Huang X L, Wang X, Zhang W T, Zhou D, Zhou Q, Liu B B and Cui T 2019 *Chin. Phys. B* **28** 096402
[11] Wang W D, Li L L, Yang C C, Soler-Crespo R A, Meng Z X, Li M L, Zhang X, Keten S and Espinosa H D 2017 *Nanotechnology* **28** 164005
[12] Ma X, Li Z Hui, Jing X L, Gu H K, Tian H, Dong Q, Wang P, Liu R, Liu B and Li Q J 2019 *Chin. Phys. B* **28** 066402
[13] Nayak A P, Bhattacharyya S, Zhu J, Liu J, Wu X, Pandey T, Jin C Q, Singh A K, Akinwande D and Lin J F 2014 *Nat. Commun.* **5** 4731
[14] Chi Z H, Zhao X M, Zhang H, Goncharov A F, Lobanov S S, Kagayama T, Sakata M and Chen X J 2014 *Phys. Rev. Lett.* **113** 036802
[15] Aksoy R, Ma Y, Selvi E, Chyu M C, Ertas A and White A 2006 *J. Phys. Chem. Solid* **67** 1914
[16] Bandaru N, Kumar R S, Sneed D, Tschauner O, Baker J, Antonio D, Luo S N, Hartman T, Zhao Y S and Venkat R 2014 *J. Phys. Chem. C* **118** 3230
[17] Jiang J J, Li H P, Dai L D, Hu H Y and Zhao C S 2016 *AIP Adv.* **6** 035214
[18] Zhuang Y K, Dai L D, Wu L, Li H P, Hu H Y, Liu K X, Yang L F and Pu C 2017 *Appl. Phys. Lett.* **110** 122103

[19] Cheng X, Li Y, Shang J, Hu C S, Ren Y F, Liu M and Qi Z M 2018 *Nano Res.* **11** 855
[20] Hromadova L, Martoňák R and Tosatti E 2013 *Phys. Rev. B* **87** 144105
[21] Fan X F, Chang C H, Zheng W T, Kuo J L and Singh D J 2015 *J. Phys. Chem. C* **119** 10189
[22] Fan X, Singh D J, Jiang Q and Zheng W T 2016 *Phys. Chem. Chem. Phys.* **18** 12080
[23] Chi Z, Chen X, Yen F, Peng F, Zhou Y H, Zhu J L, Zhang Y J, Liu X D, Lin C L, Chu S Q, Li Y C, Zhao J G, Kagayama T, Ma Y M and Yang Z R 2018 *Phys. Rev. Lett.* **120** 037002
[24] Zhao Z, Zhang H, Yuan H, Wang S B, Lin Y, Zeng Q S, Xu G, Liu Z X, Solanki G K, Patel K D, Cui Y, Hwang H Y and Mao W L 2015 *Nat. Commun.* **6** 7312
[25] Kohulák O and Martoňák R 2017 *Phys. Rev. B* **95** 054105
[26] Rifliková M, Martoňák R and Tosatti E 2014 *Phys. Rev. B* **90** 035108
[27] Duwal S and Yoo C S 2016 *J. Phys. Chem. C* **120** 5101
[28] Nayak A P, Pandey T, Voiry D, Liu J, Moran S T, Sharma A, Tan C, Chen C H, Li L J, Chhowalla M, Lin J F, Singh A K and Akinwande D 2014 *Nano Lett.* **15** 346
[29] Kim J S, Ahmad R, Pandey T, Rai A, Feng S M, Yang J, Lin Z, Terrones M, Banerjee S K, Singh A K, Akinwande D and Lin J F 2017 *2D Mater.* **5** 015008
[30] Ghorbani-Asl M, Borini S, Kuc A and Heine T 2013 *Phys. Rev. B* **87** 235434
[31] He J, Hummer K and Franchini C 2014 *Phys. Rev. B* **89** 075409
[32] Liang T, Phillpot S R and Sinnott S B 2009 *Phys. Rev. B* **79** 245110
[33] Li T 2012 *Phys. Rev. B* **85** 235407
[34] Cooper R C, Lee C, Marianetti C A, Wei X D, Hone J and Kysar J W 2013 *Phys. Rev. B* **87** 035423
[35] Zhao Y, Liao C and Ouyang G 2018 *J. Phys. D: Appl. Phys.* **51** 185101
[36] Aitken Z H and Huang R 2010 *J. Appl. Phys.* **107** 123531
[37] Sun C Q, Li C M, Bai H L and Jiang E Y 2005 *Nanotechnology* **16** 1290
[38] Chen Z, Sun C Q, Zhou Y and Ouyang G 2008 *J. Phys. Chem. C* **112** 2423
[39] Zhang A, Luo S, Ouyang G and Yang G W 2013 *J. Chem. Phys.* **138** 244702
[40] Sun C Q 2007 *Prog. Solid State Chem.* **35** 1
[41] Ouyang G, Wang C X and Yang G W 2009 *Chem. Rev.* **109** 4221
[42] Zhang A, Zhu Z M, He Y and Ouyang G 2012 *Appl. Phys. Lett.* **100** 171912
[43] Xiong S and Cao G X 2015 *Nanotechnology* **26** 185705
[44] Varshney V, Patnaik S S, Muratore C, Roy A K, Voevodin A A and Farmer B L 2010 *Comput. Mater. Sci.* **48** 101
[45] Guo H, Yang T, Tao P, Wang Y and Zhang Z D 2013 *J. Appl. Phys.* **113** 013709
[46] Chu S, Park C and Shen G 2016 *Phys. Rev. B* **94** 020101
[47] Birch F 1947 *Phys. Rev.* **71** 809
[48] Ouyang G, Sun C Q and Zhu W G 2008 *J. Phys. Chem. B* **112** 5027